Critical evaluation of the Fe−Ni, Fe−Ti and Fe−Ni−Ti alloy systems

G. Cacciamani [a,*], J. De Keyzer [b], R. Ferro [a], U.E. Klotz [c], J. Lacaze [d], P. Wollants [b]

[a] *Dip. di Chimica e Chimica Industriale, Università di Genova, I-16146 Genova, Italy*
[b] *Department of Metallurgy and Materials Engineering, Katholieke Universiteit Leuven, B-3001 Leuven, Belgium*
[c] *Empa, Materials Science and Technology, CH-8600 Duebendorf, Switzerland*
[d] *CIRIMAT, UMR CNRS/UPS/INPT 5085, ENSIACET, F-31077 Toulouse, France*

Abstract

The Fe−Ni−Ti alloy system has been evaluated, together with Fe−Ni and Fe−Ti binary subsystems, to provide reliable information for applications and in view of a thermodynamic modelling of the system. Available literature has been critically evaluated, mainly considering phase constitution and phase equilibria, thermochemical and diffusion data, as well as ab initio atomistic calculations. A discussion of the presently available CALPHAD-type thermodynamic assessments is also presented. Finally, new experimental investigations needed to solve uncertain and contradictory data are suggested.

Keywords: A. Ternary alloy systems; A. Intermetallics; B. Phase diagrams; B. Crystallograpy; B. Thermodynamic and thermochemical properties

1. Introduction

This paper is part of a more extensive study of the Al−Fe−Ni−Ti quaternary system, the core objective of the European project COST 535 ''Thalu'' (thermodynamics of alloyed aluminides).

The by far most important technical applications for Fe- and Ni-based alloys are of course steels and super alloys [1]. Additions of up to 2 wt% of Ti are important in steels to form carbides, as grain refining element or to enhance oxidation resistance. In Ni-based super alloys up to 5 wt% of Ti is used to form the γ' phase. However, the properties of these alloy classes are controlled by the combined influences of all elements, which sometimes exceed the number 10. Materials more focused on the Fe−Ni−Ti system are complex metallic alloys such as shape memory alloys, bulk metallic glasses, quasicrystals or hydrogen storage intermetallic compounds.

* Corresponding author. Dip. di Chimica e Chimica Industriale, Università di Genova, via Dodecaneso 31, I-16146 Genova, Italy. Tel.: +39 010 353 6152; fax: +39 010 362 5051.
E-mail address: cacciamani@chimica.unige.it (G. Cacciamani).

Shape memory alloys are metallic materials showing a stress induced diffusionless phase transformation from a high temperature phase into the low temperature phase [2]. Several authors contributed to this subject and their results have been summarized in the review by Guerin [3], though this is still an active field of investigation [4−7]. Typical shape memory alloys are based on NiTi alloys having a composition of 55−55.5 wt% Ni (45−45.5 wt% Ti) with small additions of Co or Al [8]. Small Al additions to NiTi result in the formation of an intermediate phase in thermal cycles, having a beneficial effect on shape memory properties [9].

Iron containing shape memory alloys are based on Fe−Mn−Si−Ni−Cr [10] or Fe−Co−Ni−Ti alloys [11]. Typical applications are not only in medicine, for instance surgery instruments or endoscopes, but also in construction industry as fasteners or pipe joints. More recent overviews about the status of development, properties, applications and characterization methods of shape memory alloys are available [12−15]. Thermodynamic modelling can be applied in order to determine alloy properties decisive for good shape memory properties [16].

Bulk metallic glasses (BMG) are formed in various alloy systems [17]. Interesting examples in the present context are

doi:10.1016/j.intermet.2005.11.028

the (Fe,Ni)−(Zr−Hf−Nb)−B, Ni−Zr−Ti−Sn−Si, Ti−Ni−Cu−Sn and Ti−Zr−Fe systems. Important factors controlling the glass forming ability are (i) a multicomponent system consisting of more than three elements, (ii) a significant atomic size mismatch above 12% and (iii) a negative heat of mixing. The importance of reliable thermodynamic and structural data for alloy development is therefore obvious. Technical applications of BMG are driven by their extreme mechanical and physical properties, for instance high strength exceeding 2 GPa, low damping, high corrosion resistance or special magnetic properties [17,18].

Heusler phases are intermetallic phases based on the prototype Cu_2MnAl and show ferromagnetic behaviour though not containing Fe, Ni or Co. They also form in other alloying systems such as Ni_2AlX (X = Ti, Cr, V, Mn) or X_2AlTi (X = Fe, Co, Ni, Cu) and show some interesting physical properties due to their electronic structure such as semiconductivity [19], thermoelectricity [20] and magnetic properties [21]. This might be interesting for new technical applications in these fields. Heusler phases, while not present in Fe−Ni−Ti, are relevant in other Al−Fe−Ni−Ti subsystems.

Quasicrystals were discovered in 1984 in the Al−Mn system and are characterized by a non-periodic lattice, however, showing long-range order. They form in several alloying systems, among which Ti−Zr−Ni [22] and Ti−Ni−Fe−Si [23] are of special interest. Their atomic structure results in interesting mechanical properties such as high hardness and elasticity coupled with reasonable ductility, as well as in exceptional electronic properties. These properties are already applied in quasicrystalline coatings with high abrasion resistance and might be used in thermoelectricity in future.

Technical applications of hydrogen storage materials have been found in Ni metal hydride (Ni-MH) batteries since the 1990s. Upcoming applications are hydrogen tanks for fuel cell cars because of their compactness and safety for hydrogen energy storage. Metallic materials for hydrogen storage are either hydride forming transition metals MH_n ($n = 1, 2, 3$), metallic hydrides of intermetallic compounds AB_xH_n ($x = 0.5, 1, 2, 5$) or complex hydrides forming an ionic or covalent compound upon hydrogen absorption [24,25]. Fe−Ni−Ti system compounds with high hydrogen absorption are FeTi with partial substitution of Fe with Ni [26,27] and Ti_2Ni [25].

Phase changes during mechanical deformation in Fe−Ni−Ti have been investigated by Sagaradze et al. [28,29]. They obtained both $AuCu_3$-type and Ni_3Ti-type structures from mechanical alloying of the Fe−Ni−Ti fcc solid solution and observed their dissolution during cold deformation between 20 and −196 °C.

2. Binary subsystems

2.1. Fe−Ni

A comprehensive evaluation of the Fe−Ni phase diagram was carried out by Swartzendruber et al. [30] including references up to 1989. Solid state equilibria were discussed previously by Rossiter and Jago [31]. The presence of a miscibility gap, induced in the gamma phase by the magnetic transition, was suggested by CALPHAD-type thermodynamic calculations [32,33] and subsequently confirmed by experimental investigations [34] on stable and metastable equilibria in meteoritic samples in the 200−700 °C temperature range (Figs. 1 and 2). According to Yang et al. [34] a monotectoid equilibrium $\gamma\text{-(Fe,Ni)}_{\text{param}} = \gamma\text{-(Fe,Ni)}_{\text{ferrom}} + \alpha\text{-Fe}$ occurs at about 415 °C and $\gamma\text{-(Fe,Ni)}_{\text{ferrom}}$ decomposes eutectoidally into α-Fe and $FeNi_3$ at about 345 °C. Both Rossiter and Jago [31] and Yang et al. [34] considered as metastable an FeNi phase with the $L1_0$, AuCu-type structure, reported as a stable phase by Reuter et al. [35]. They also agreed that phase relations at lower temperatures can hardly be explored because thermodynamic equilibrium cannot be achieved below 200 °C, even at geological time scale.

The martensitic transformation occurring in the Fe-rich part of the system was investigated by several authors: see for instance Kakeshita et al. [36] and references therein. High pressure equilibria in the Fe-rich part have been studied by Mössbauer spectroscopy [37]. A metastable Fe_3Ni phase with $L1_2$ superstructure was observed by Munroe and Hatherly [38] in meteoric samples.

Thermodynamic data up to 1989 have been reviewed by Swartzendruber et al. [30]. The most interesting original references are cited in Table 1. Although some references to specific heat evaluations were listed in this review, measurements of Hausch [64] and references therein were not mentioned. Later Seifter et al. [65] measured the enthalpy and some physical properties of Fe−Ni alloys in a temperature range from room temperature to 2400 K.

More recently the enthalpy of mixing at concentrations up to 46 at.% Ni at 1900 K and up to 25 at.% Fe at 1913 K was measured by Thiedemann et al. [44] using levitation drop calorimetry. The results agree reasonably well with previous data [43,42,40] as shown in Fig. 3. A minimum of about −5 kJ/mol at $x_{Ni} = 0.6$ is indicated. Thiedemann et al. [44] could also describe their results using an equation according to the modified quasichemical solution model.

Thermodynamic measurements for the energy difference between the austenite and the martensitic phases in Fe−Ni were carried out by Chang et al. [66] and Rostovtsev et al. [67] and references therein.

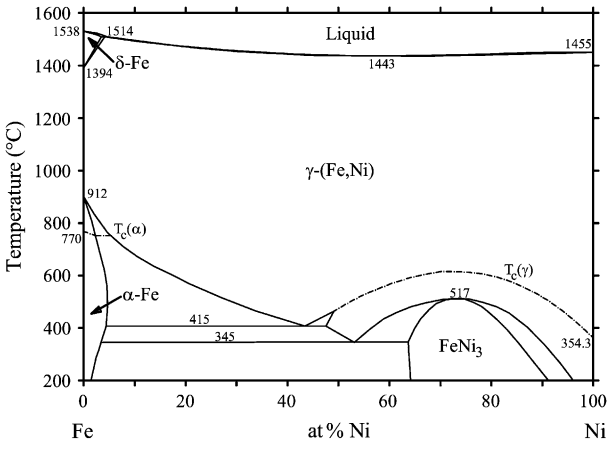

Fig. 1. The assessed Fe−Ni phase diagram.

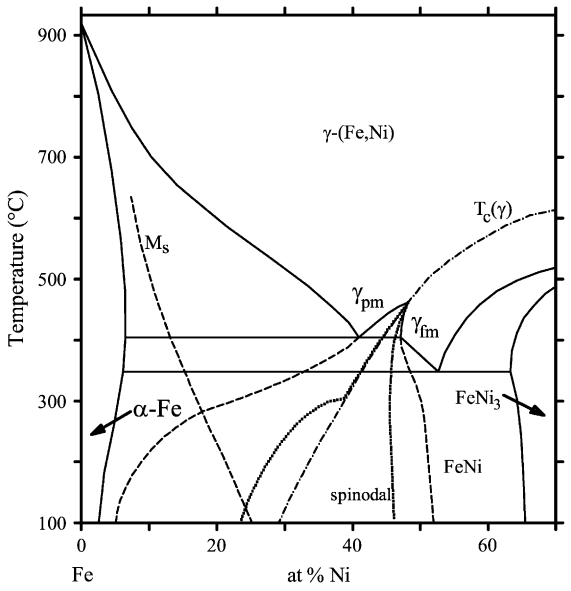

Fig. 2. Metastable equilibria in the Fe−Ni phase diagram according to Yang et al. [34]. M_s: martensitic transformation start temperature; γ_{pm}, γ_{fm}: paramagnetic and ferromagnetic disordered gamma phases. The metastable continuation of the miscibility gap is represented by dashed lines. The spinodal region inside the miscibility gap is also shown. At lower temperatures γ_{fm} assumes the ordered $L1_0$ (FeNi) structure (transformation equilibria are not determined).

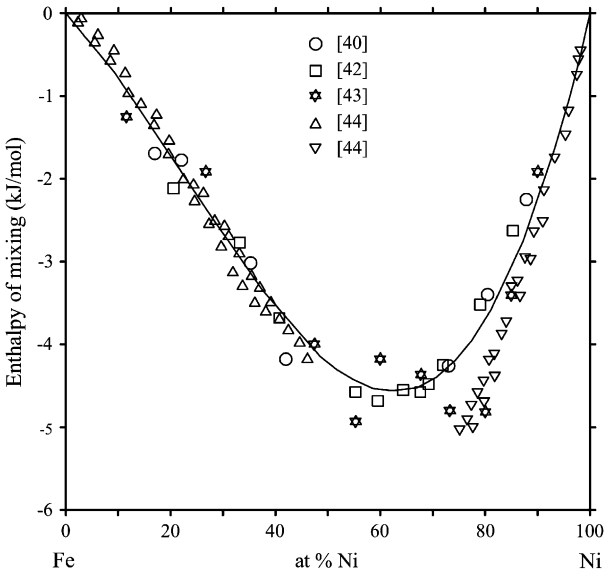

Fig. 3. Enthalpy of mixing for liquid Fe−Ni alloys. Data points from Predel and Mohs [40], Batalin et al. [42], Iguchi et al. [43] and Thiedemann et al. [44]; computed line according to Lee [72].

Initial CALPHAD-type thermodynamic assessments [32,68,33] have been improved by Lee and Lee [69], who described the ordered $FeNi_3$ phase and the disordered fcc phase as one phase, and re-optimised the liquid parameters. Subsequently Ohnuma et al. [70,71], re-modelled the magnetic contribution to the Gibbs energy of the ordered $FeNi_3$ phase. The $L1_0$ FeNi phase, which appeared to be stable in the first paper [70], was no more present in the latter one [71]. The assessment by Lee [72], reported in Fig. 4, has to be considered as a starting point for further improvements such as: the 4-sublattice modelling of the fcc phases and the addition of the magnetic parameters for the description of the ordered $FeNi_3$ phase [70].

In an independent thermodynamic calculation of the Fe−Ni phase equilibria recently published by Howald [73] the $L1_0$ FeNi phase results to be stable in the 100−250 °C temperature range. It has to be mentioned, however, that this cannot be considered as a true assessment because most of the recent Fe−Ni literature is not considered.

The boundaries of the $L1_2$ disordered phase were calculated phenomenologically using a computational approach based on the cluster variation method (CVM) with a tetrahedron nearest neighbour approximation for the fcc structure and combined with Lennard-Jones (L-J) type pair potentials [74]. The calculated boundaries agree reasonably with the experimental lines. In a similar way the existence of the tetragonal FeNi phase, not present in conventional phase diagrams, was simulated. According to these calculations the $L1_0$ phase should be stable, but experimental verification is necessary.

In agreement with the experimental observations, Mishin et al. [75] found, by first principles calculations using the linearised augmented plane wave method in the generalized gradient approximation that the $L1_2$-Ni_3Fe compound is the most stable one. They found that the $L1_0$ FeNi phase is metastable but close to being stable. According to their calculations the previously unknown C11 compounds Fe_2Ni and Ni_2Fe are expected to be stable.

The influence of magnetic interaction on the order−disorder transition temperature in Fe_3Ni, FeNi and $FeNi_3$

Table 1
References on thermochemical data concerning the Fe−Ni binary system

Measured quantities	References
Heat of mixing for liquid alloys	[39−44]
Heat of mixing for solid alloys	[45−48]
Activity coefficients for Ni in liquid	[49−57]
Activity coefficients for Fe in liquid	[50,49,52−57]
Activity coefficients for Ni in γ-(Fe,Ni)	[58−63,55,57]
Activity coefficients for Fe in γ-(Fe,Ni)	[58−63,55,57]

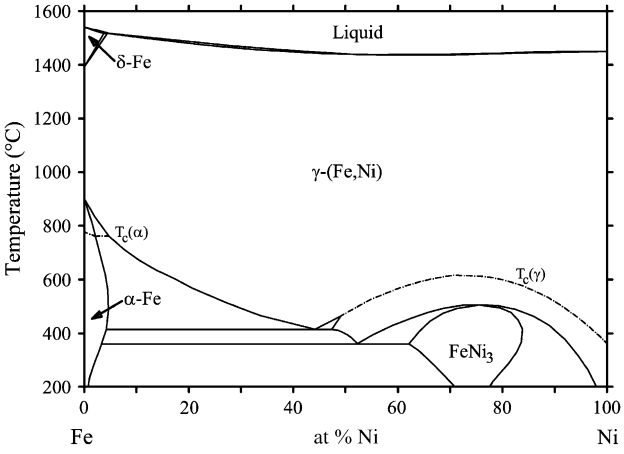

Fig. 4. The computed Fe−Ni phase diagram according to the update by Lee [72]. Computed invariant temperatures are not given in the original paper. Phase equilibria may be compared to Fig. 1.

was studied by Rancourt et al. using both mean field theory [76,77] and Monte Carlo simulations, combined with an Ising Hamiltonian [78]. They concluded that magnetic interactions, although much weaker than the chemical bond energies, must be included and that mean field theory cannot be used for either the magnetic interactions (due to magnetic frustration and magnetic short-range order) or the chemical degrees of freedom (chemical short-range order is not described).

The diffusion in the Fe−Ni system was modelled by Jönsson [79]. A CALPHAD-type procedure was used to assess the atomic mobilities as a function of temperature and composition. In this article most of the literature on diffusion data up to 1986 was reviewed. More recently Ugaste et al. [80] studied the compositional dependence of the interdiffusion coefficient at 1100 °C using the Matano−Boltzmann technique.

2.2. *Fe−Ti*

The phase diagram shown in Fig. 5 results from the critical evaluation by Murray [81] which only contains bibliographic information up to 1981. Since then, a limited number of new phase diagram data have become available: a new investigation of the A2/B2 boundary in the Ti-rich corner [82], the study of the retrograde solubility of Fe in α-Ti by Mössbauer spectroscopy [83], the determination of the high pressure equilibria in the Fe-rich [84] and Ti-rich [85] sides of the phase diagram. Formation of quasicrystals was discovered in rapidly solidified $FeTi_2$ samples [86]. Jonsson [87] reported an overview of the available information on thermodynamic data. The references to the different original papers are included in Table 2, though one of the more recent measurements [99] was not listed in his review. Thiedemann et al. [99] measured the enthalpies of mixing using levitation alloying calorimetry at concentrations up to 42 at.% Ti at 1950 K and 31 at.% Fe at 2112 K. The results, shown in Fig. 6, are the only measurements performed till now at high-Ti concentrations. Assuming that FeTi associates are formed, the authors could describe their results using the regular associate model. Based on these measurements Qin et al. [100] derived the activities and partial Gibbs energies for Fe and Ti.

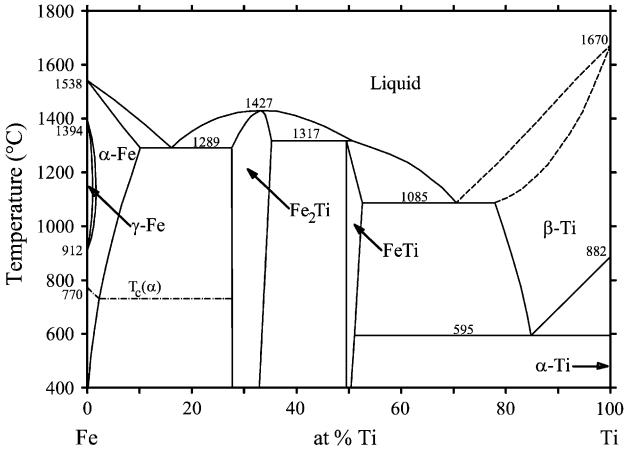

Fig. 5. The assessed Fe−Ti phase diagram according to Murray [81].

Table 2
References on thermochemical data concerning the Fe−Ti binary system

Measured quantities	Phase	References
Heat of formation	FeTi	[88]
Activity of Ti	Liquid	[89]
Partial excess Gibbs energies	Liquid	[90]
Activity of Ti and Fe	Liquid	[91]
Partial enthalpy of mixing	Liquid	[92]
Heat of formation	FeTi and Fe_2Ti	[93,94]
Enthalpy of mixing	Liquid	[95]
Heat of formation	FeTi and Fe_2Ti	[96]
Enthalpy of mixing	Liquid	[97]
Heat capacity	FeTi and Fe_2Ti	[98]
Enthalpy of mixing	Liquid	[99]

A first CALPHAD-type assessment of the Fe−Ti system was performed in 1978 by Kaufman and Nesor [101]. Since then several new CALPHAD-type assessments have been carried out [102,96,81,103−105,87,106] and compared by Dumitrescu et al. [106]. More recently, two more assessments were achieved by Hari Kumar [107] and Balun [108]. Hari Kumar used a 3-sublattice model for the FeTi-B2 phase, thus allowing for the description of its homogeneity range which was not described in the previous works. The Gibbs energy of this phase was coupled with the Gibbs energy of the disordered bcc phases (A2) that are found on both the Ti- and Fe-rich sides, in order to describe the disorder−order transformation between the disordered phase and the ordered FeTi-phase. Also the magnetic contribution to the Gibbs energy of the A2 phase was included. Balun [108] has recently performed a similar optimisation, which appears in slightly lower agreement with experimental data. The assessment by Hari Kumar is thus recommended and the corresponding phase diagram is shown in Fig. 7 while the optimised enthalpy of mixing is shown in Fig. 6.

The ordering between A2 and B2 is one of the main features of this diagram. Apart from the many CALPHAD-type

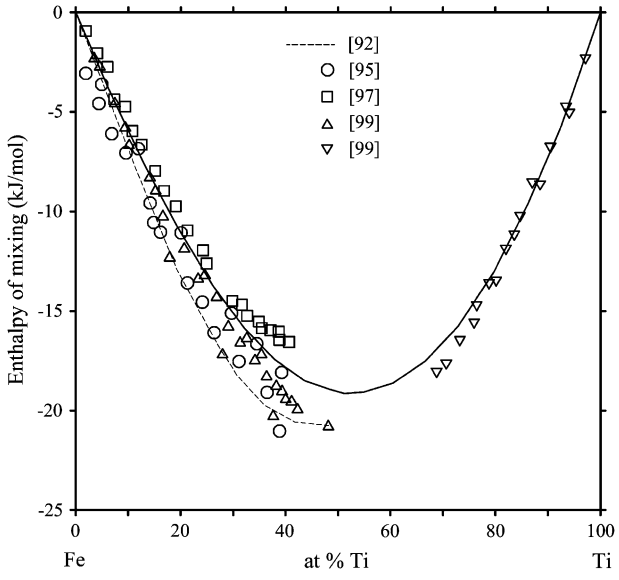

Fig. 6. Enthalpy of mixing for liquid Fe−Ti alloys. Data points from Esin et al. [92], Batalin et al. [95], Wang et al. [97] and Thiedemann et al. [99]; calculation (full line) according to Hari Kumar [107].

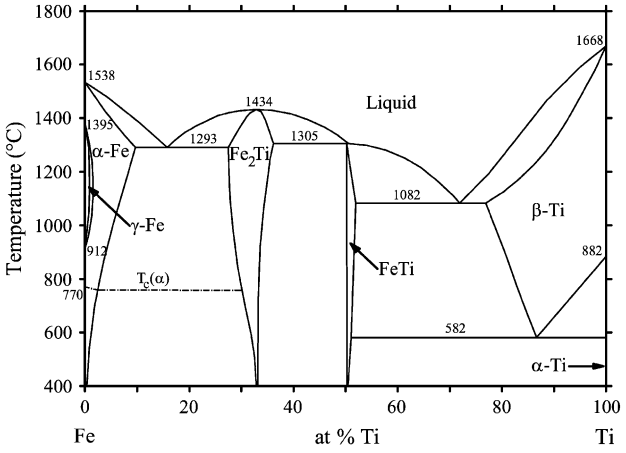

Fig. 7. The computed Fe—Ti phase diagram according to Hari Kumar [107].

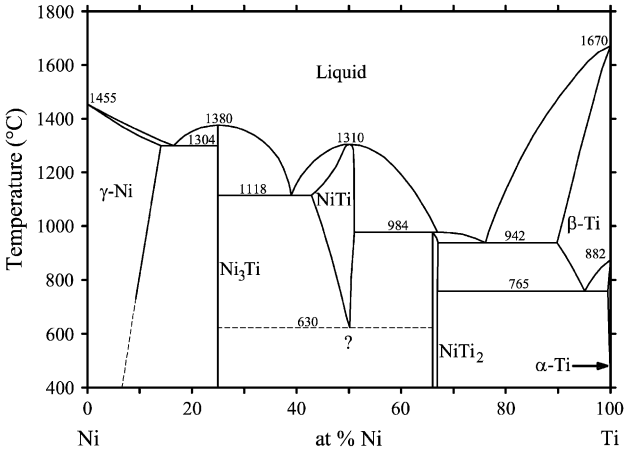

Fig. 8. The assessed Ni—Ti phase diagram according to Murray [123].

assessments, some other calculations can also be found trying to describe the equilibrium between these phases. Inden [109] estimated the interchange energies between the nearest and the next-nearest neighbour atoms based on enthalpies of formation of the bcc alloys and the two-phase equilibrium between the ordered and disordered phases on the Ti-rich side of the phase diagram. Using the cluster variation method, Ohnuma et al. [110] fitted interaction terms for the second nearest neighbour pairs and for the tetrahedron interaction terms based on the titanium rich side of the Al—Fe—Ti phase diagram. More recently, Eleno et al. [111] derived new values for the pair interactions between first and second nearest neighbours and for the tetrahedron correction terms.

The diffusion of Fe in β-Ti as well as in α-Ti is known to be very fast [112]. The diffusivity of Fe in α-Ti was found to be in the range of 10^{-14}—10^{-11} m^2/s at temperatures from 900 to 1100 K, which is almost 10^5 times larger than the self-diffusion of Ti [113]. The diffusion is anisotropic and larger in the direction parallel to the *c*-axis [112]. The diffusion of Fe in β-Ti was studied using Mössbauer spectroscopy [114]. The diffusivity was found to be in the range of 10^{-13}—10^{-11} m^2/s at temperatures from 1100 to 1400 K and to be reduced by the addition of Fe, which was interpreted to be due to short-range ordering of Fe atoms in the alloys. Diffusion coefficients were also determined by the Hall's method [115] and similar values were found. Efimenko et al. [116], however, found values for the interdiffusion of Fe and Ti that are about 10 times smaller. Yoshida [117] used Mössbauer spectroscopy to determine the elementary diffusion jumps of Fe in β-Ti, but no definite jump model could be proposed. Diffusion of Ti in α-Fe ranges from 10^{-18} to 10^{-14} m^2/s at temperatures from 950 to 1200 K and is faster by a factor of 5 when compared to Fe self-diffusion (see Klugkist and Herzig [118] and references therein). Diffusion was also studied extensively in the light of joints of titanium to stainless steel and Inconel [119—122].

2.3. Ni—Ti

Ni—Ti binary subsystem has not been reviewed in this work. It is here provisionally accepted as presented and evaluated by Murray [123] (Fig. 8). The most recent CALPHAD-type thermodynamic assessment is due to Bellen et al. [124] (Fig. 9).

3. Fe—Ni—Ti phases

No ternary phase is present in the Fe—Ni—Ti system whilst binary Ni_3Ti, $NiTi_2$ and Fe_2Ti phases show large solubility of the third element and form homogeneous fields extending into the ternary at almost constant Ti content. $NiTi_2$ dissolves so much Fe that its solubility range extends very close to the Fe—Ti binary as shown in the 900 °C isothermal section presented below. It is, however, incomplete, no $FeTi_2$ compound being stable in the Fe—Ti system. NiTi and FeTi are isostructural (B2-CsCl type) and form a continuous solid solution crossing the phase diagram at about 50 at.% Ti. Close to the Fe—Ni binary subsystem the γ-(Fe,Ni) solid solution dissolves a few at.% of Ti. The variation of the lattice parameter with the Ti concentration has been studied by Abraham [125] in two series of alloys at 27 and 29.75 at.% Ni, respectively. In both series a non-linear trend was observed with a minimum at about 2.5 at.% Ti. It was interpreted as a consequence of an ordering effect in which Ni and Ti positions in the fcc matrix are correlated. In selected samples, moreover, broadened peaks were observed and broadening was interpreted as

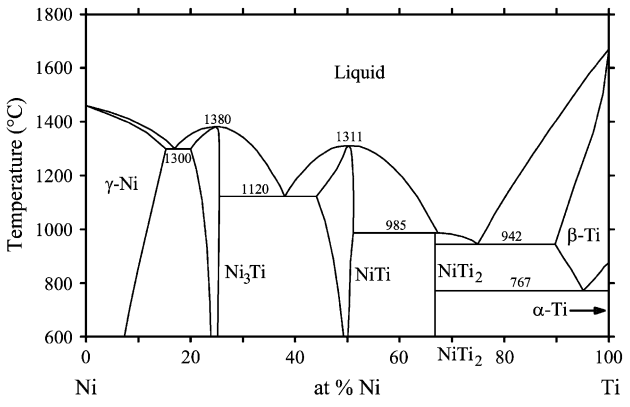

Fig. 9. The calculated Ni—Ti phase diagram according to Bellen et al. [124].

possibly related to the presence of two different (ferro- and anti-ferromagnetic) fcc phases with slightly different lattice parameters. Structural data of the binary phases and their extension in the ternary system are summarized in Table 3.

The low temperature structural transformations producing the well-known shape memory effect in NiTi are affected by Fe additions and several investigations have been performed, most often on $Fe_xNi_{50-x}Ti_{50}$ alloys with x in between 0 and 3 [130–137,128,138,139,4–7]. The martensitic transformation of B2 to monoclinic B19″ (sometimes denoted by M), with $M_s = 60–70$ °C in the binary NiTi system, is strongly affected by the addition of a third element. Fe, which substitutes Ni in the B2-NiTi structure, leads to a lowering of the M_s temperature and causes a two-stage transformation: B2 to R to M. Typically, M_s is lowered to about −80 °C while the R-phase (the same phase observed in Ni-rich B2-NiTi alloys) occurs at about 0 °C in a $Fe_3Ni_{47}Ti_{50}$ alloy. The temperature hysteresis is about 30–40 °C for the martensitic transformation and only 2–5 °C for the B2 to R transition. According to the recent neutron diffraction investigations by Voronin et al. [6] a triclinic instead of monoclinic structure was proposed for the low temperature martensite. It was observed, however, that the same diffraction results could be due to a mixture (though in unlikely proportions) of the R and M phases.

4. Fe–Ni–Ti phase diagram

The Fe–Ni–Ti phase diagram has been investigated by a few authors and was reviewed by Gupta [140,141] who also revised his own evaluation recently [142]. Vogel and Wallbaum [143,144] used thermal analysis and optical microscopy to study the binary Ni–Ti phase diagram in the range of 0–30 at.% Ti, and 11 partial isopleths in the low-Ti part of the ternary system, delimited by Fe, Ni, Ni_3Ti and Fe_2Ti. Dudkina and Kornilov [127] investigated the isopleth at 50 at.% Ti up to the solidus line by thermal analysis, optical microscopy, X-ray diffraction and hardness measurements. They examined 21 alloy samples produced by levitation melting from iodide titanium, electrolytic Ni and 99.94 wt% pure Fe.

Van Loo et al. [126] determined the 900 °C isothermal section by analyzing (by optical and electron microscopies, EPMA and X-ray diffraction) 15 diffusion couples and 24 equilibrated samples in the whole composition range. They used 99.95–99.99 wt% pure elements and gave detailed description of the experimental procedures and results. Abramycheva et al. [145] investigated the isothermal section at 1000 °C by using the same experimental techniques. Six diffusion couples and a number of equilibrated samples were analyzed, mainly in the region at $x(\mathrm{Ti}) < 0.5$. Their results are fairly consistent with those by Van Loo et al. [126] at 900 °C.

Alisova et al. [146] studied three isopleths in the Ti-rich (>50 at.% Ti) part of the diagram and determined the sequence of invariant equilibria and monovariant lines in this region. About 12 samples per section were prepared from iodide, Ti and Fe and Ni of undetermined purity. After appropriate heat treatments they were examined by X-ray, thermal analysis and metallography. A reaction scheme and three isopleths were drawn by Alisova et al., but no individual experimental result was reported. Other studies, though less extensive, on the Fe–Ni–Ti phase equilibria are available [147,125,148,149].

4.1. Liquidus and solidus

Experimental data concerning the liquidus surface can be derived from the isopleths investigated by Vogel and Wallbaum [143] in the Fe–Ni–Ni_3Ti–Fe_2Ti region and by Alisova et al. [146] in the Ti–FeTi–NiTi region. Their results, which may be questionable at low temperature, when solid state equilibria are involved, seem more reliable at high temperature and, in particular, as far as the liquidus curves are concerned. They have been used, together with the accepted liquidus lines of the binary systems, to draw the liquidus surface projection reported in Fig. 10. No experimental information being available in the Ni_3Ti–Fe_2Ti–FeTi–NiTi region, isothermal and monovariant curves have been only schematically drawn by interpolation between the neighbouring regions.

Dudkina and Kornilov [127] determined the solidus curve along the FeTi–NiTi section. It shows a minimum (∼1270 °C) at about equiatomic Fe/Ni ratio implying a corresponding minimum at the same composition in the liquidus curve, in contradiction with the liquidus curve they proposed. Such a concave shape of the liquidus surface along the FeTi–NiTi section may be supported by the corresponding concavity shown by the liquidus line along the Fe–Ni binary subsystem and by the same trend resulting in the low-Ti part of the diagram from the sections investigated by Vogel and Wallbaum [143].

Uncertainties still subsist about the nature, temperature and position of the invariant equilibrium involving Liquid, β-Ti, $NiTi_2$ and B2-(Fe,Ni)Ti. According to Alisova et al. [146] it is U-type, at 960 °C, and very close to the $L \rightarrow \beta\text{-Ti} + NiTi_2$ binary eutectic. However, according to the high Fe solubility in the $NiTi_2$ phase reported in the isothermal sections at 900 and 1000 °C, both temperature and phase compositions should be different. In particular, according to Abramycheva et al. [145], the $(Fe,Ni)Ti_2$ phase is stable at 1000 °C close to the Fe–Ti binary subsystem. No equilibrium between $(Fe,Ni)Ti_2$ and liquid was experimentally observed while the three phase field $\beta\text{-Ti} + NiTi_2 + \text{B2-(Fe,Ni)Ti}$ was found to be stable at this temperature. This implies that the primary solidification range of $(Fe,Ni)Ti_2$ must be substantially extended and that the invariant composition of liquid is not so close to the Ni–Ti binary as proposed by Alisova et al. [146]. If this is the case a P-type invariant $L + \beta\text{-Ti} + \text{B2-(Fe,Ni)Ti} \rightarrow (Fe,Ni)Ti_2$ may occur, or a U-type $L + \text{B2-(Fe,Ni)Ti} \rightarrow \beta\text{-Ti} + (Fe,Ni)Ti_2$ associated with a maximum in the monovariant liquidus line connecting it with the binary peritectic $L + \text{B2-NiTi} \rightarrow NiTi_2$. The latter option is compatible with a new experimental investigation by Riani et al. [150] of the phase equilibria involving $(Fe,Ni)Ti_2$.

4.2. Isothermal and isopleth sections

The FeTi–NiTi vertical section is an almost pseudobinary section (not exactly, because FeTi forms peritectically from

Table 3
Fe−Ni−Ti solid phases and lattice parameters

Phase name	Pearson symbol and prototype	Space group	Struktur-bericht design	Temperature range (°C)	Composition range	Lattice parameters[a] (nm)	References and comments
γ-(Fe,Ni)	cF4-Cu	$Fm\bar{3}m$	A1	Fe: 1394−912 Ni: <1455	Fe−Ni: Complete solubility Fe−Ti: 0−0.8 at% Ti (γ loop) Ni−Ti: 0−13.7 at% Ti	$a = 0.36467$ $a = 0.35232$ $a = 0.3575$ $a = 0.294$ $a = 0.35568$ $a = 0.3590$ $a = 0.3652$ $a = 0.35939$ $a = 0.35913$ $a = 0.35890$ $a = 0.35837$	pure Fe pure Ni $Fe_{50}Ni_{50}$ $Fe_{80}Ti_{20}$ $Ni_{90.6}Ti_{9.4}$ $Fe_{31}Ni_{63}Ti_6$, room T [126] $Fe_{31}Ni_{63}Ti_6$, 900 °C [126] $Fe_{64.4}Ni_{29.6}Ti_{6.0}$ [125] $Fe_{68.3}Ni_{26.9}Ti_{4.8}$ [125] $Fe_{68.3}Ni_{30.4}Ti_{1.3}$ [125] $Fe_{71.7}Ni_{27.1}Ti_{1.2}$ [125]
α-Fe, δ-Fe	cI2-W	$Im\bar{3}m$	A2	Fe: 1538−1394 and <912	Fe−Ni: 0−3 at% Ni at 1514 °C 0−5 at% Ni at ∼500 °C	$a = 0.28665$	pure Fe at room T
β-Ti				Ti: 1670−882	Fe−Ti: 0−10 at% Ti 0−22 at% Fe Ni−Ti: 0−10 at% Ni	$a = 0.33065$ $a = 0.3224$	pure Ti $Ni_{9.5}Ti_{90.5}$ [126]
(Fe,Ni)Ti	cP2-CsCl	$Pm\bar{3}m$	B2	FeTi: <1317 NiTi: <1311	Fe−Ti: 49.7−52.5 at% Ti Ni−Ti: 43−50.5 at% Ti Fe−Ni−Ti: Complete solubility between FeTi and NiTi	$a = 0.29789$ $a = 0.29818$ $a = 0.29891$ $a = 0.3000$ $a = 0.3010$ $a = 0.2985$	$Fe_{50}Ti_{50}$ $Fe_{35.3}Ni_{14.7}Ti_{50}$ [127] $Fe_{25.3}Ni_{24.7}Ti_{50}$ [127] $Fe_{10.2}Ni_{39.8}Ti_{50}$ [127] $Ni_{52}Ti_{48}$ $Fe_{25}Ni_{25}Ti_{50}$
R-phase (pre-martensite)	hR18	$P3$	—	0 to −80 at 3 at% Fe	Fe−Ni−Ti: 5 at% Fe, ∼50 at% Ti	$a = 0.73580$ $c = 0.52855$	$Ni_{50.23}Ti_{49.77}$ [4]
B19'' (martensite)	mP4	$P2_1/m$	—	NiTi: <∼60 <−80 at 3 at% Fe	Fe−Ni−Ti: 5 at% Fe, ∼50 at% Ti	$a = 0.2898$ $b = 0.4108$ $c = 0.4646$ $\beta = 97.78°$	[128]
	aP24	$P1$	—			$a = 0.5588$ $b = 1.3762$ $c = 0.5110$ $\alpha = 72.83°$ $\beta = 73.39°$ $\gamma = 73.52°$	[6]
α-Ti	hP2-Mg	$P6_3/mmc$	A3	Ti: <882	Fe−Ti: <0.04 at% Fe Ni−Ti: <0.2 at% Ni	$a = 0.29506$ $c = 0.46825$	pure Ti
$FeNi_3$	cP4-$AuCu_3$	$Pm\bar{3}m$	$L1_2$	<517	Fe−Ni: 63−∼85 at% Ni Ti solubil. not known	$a = 0.35523$	[30]
Fe_2Ti (Laves phase)	hP12-$MgZn_2$	$P6_3/mmc$	C14	<1427	Fe−Ti: 27.6−35.2 at% Ti Fe−Ni−Ti: 0−30 at% Ni.	$a = 0.4785$ $c = 0.7799$ $a = 0.4956$ $c = 0.8032$	$Fe_{66.7}Ti_{33.3}$ $Fe_{33.9}Ni_{33.0}Ti_{33.1}$

(*continued on next page*)

Table 3 (*continued*)

Phase name	Pearson symbol and prototype	Space group	Struktur-bericht design	Temperature range (°C)	Composition range	Lattice parameters[a] (nm)	References and comments
Ni_3Ti	hP16-$TiNi_3$	$P6_3/mmc$	DO_{24}	<1380	Ni–Ti: 20–25 at % Ti Fe–Ni–Ti: 0–20 at % Fe	$a = 0.51088$ $c = 0.83187$	$Ni_{75}Ti_{25}$
						$a = 0.5103$ $c = 0.8320$	$Fe_4Ni_{71}Ti_{25}$ [126]
$NiTi_2$	cF96	$Fd\bar{3}m$	$E9_3$	<984	Ni–Ti: 66–67 at % Ti Fe–Ni–Ti: 0–30 at % Fe.	$a = 1.13193$ $a = 1.1338$ $a = 1.1324–1.1350$	at 19 at % Fe 0–26.7 at % Fe [129]

[a] Unless different references are given, lattice parameters are reported from Villars et al. [161].

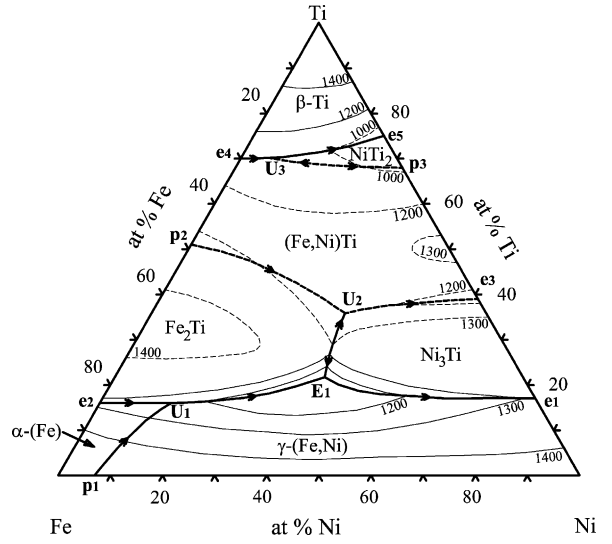

Fig. 10. Fe–Ni–Ti liquidus projection. Dashed lines represent interpolated or uncertain equilibria.

Liquid and Fe_2Ti phases). A second vertical section, Ni_3Ti–Fe_2Ti, was considered as pseudobinary though the Ni_3Ti–Fe_2Ti tie-lines are not exactly in the section, due to the extension of the solubility ranges of the two phases. These two sections, FeTi–NiTi and Ni_3Ti–Fe_2Ti, divide the phase diagram into three fields, which will be described in the following.

4.2.1. The high-Ti region (x(Ti) > 0.5)

Main investigations in this region have been performed by Van Loo et al. [126] (isothermal section at 900 °C, Fig. 11), Abramycheva et al. [145] (partial isothermal section at 1000 °C, Fig. 12) and Alisova et al. [146] who determined three vertical sections at 1/3, 1/1 (reported in Fig. 13) and 3/1 Fe/Ni ratios. The three works agree in the description of

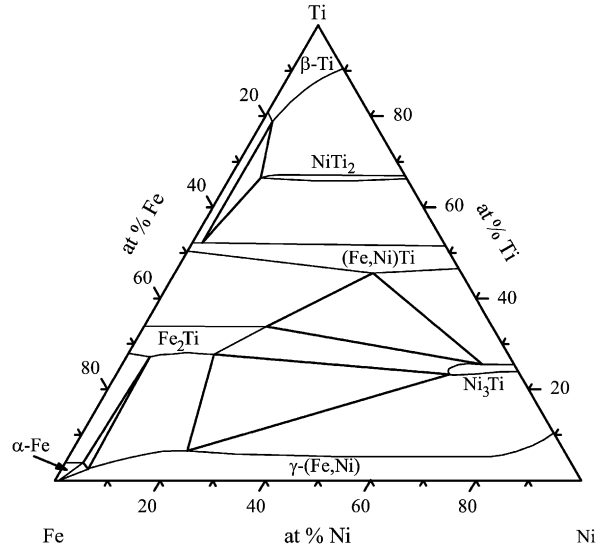

Fig. 11. Fe–Ni–Ti isothermal section at 900 °C according to Van Loo et al. [126].

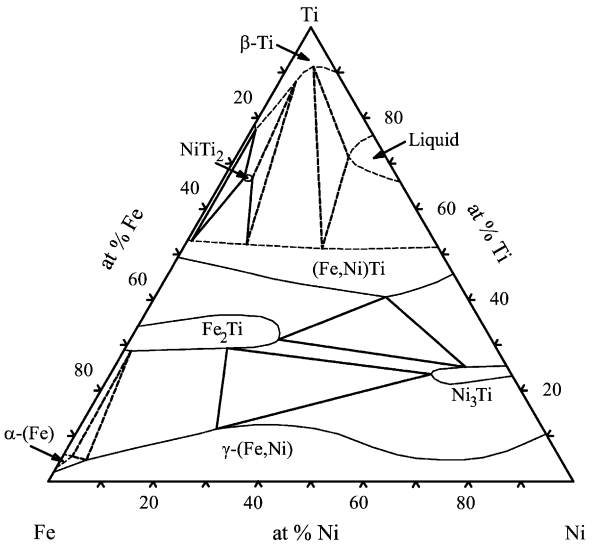

Fig. 12. Fe−Ni−Ti isothermal section at 1000 °C according to Abramycheva et al. [145].

the B2-(Fe,Ni)Ti solid solution: it is complete, from NiTi to FeTi and Ti solubility is not exceeding 52−54 at.% Ti, depending on temperature and Fe/Ni ratio. According to Van Loo et al. [126] and Abramycheva et al. [145], $NiTi_2$ dissolves a large amount of Fe and a three phase field B2-(Fe,Ni)Ti + (Fe,Ni)Ti_2 + β-Ti is present close to the Fe−Ti binary subsystem. Equilibrium phase compositions indicated by the two authors are in good agreement, as can be seen in Table 4.

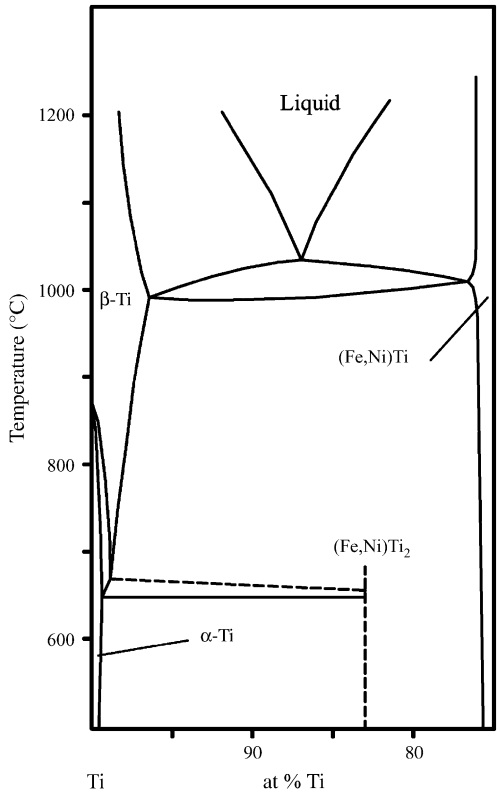

Fig. 13. Fe−Ni−Ti partial vertical section at Fe/Ni equiatomic ratio according to Alisova et al. [146]. See text for discussion.

According to Alisova et al. [146], however, $NiTi_2$ does not dissolve more than a few at.% Fe and shows up only in the vertical section closest to the Ni−Ti side. The results by Van Loo et al. [126], also confirmed by Riani et al. [150], are here considered more reliable because the experimental procedures and results are very well described and exhaustively discussed. The three-phase equilibrium, in particular, is supported by one diffusion couple and two equilibrated samples. One of the three sections proposed by Alisova et al. [146] has been reproduced in Fig. 13. Van Loo et al. [126] and Alisova et al. [146] also disagree about the extent and shape of the β-Ti homogeneity range. According to the former authors the solubility range of β-Ti at 900 °C gradually increases with the Fe/Ni ratio from about 10 at.% Ni in Ni−Ti to about 20 at.% Fe in Fe−Ti. On the contrary, according to Alisova et al. [146], it decreases in both cases when the third element is added and, at 900 °C, it reaches a minimum of about 95 at.% Ti at Fe/Ni equiatomic ratio. Finally, the (β-Ti)−(α-Ti) two-phase equilibria shown in the three vertical sections by Alisova et al. [146] can be hardly reconciled with the accepted binary equilibria. As an example, the β-Ti monovariant line connecting the binary eutectoidic equilibria at 85 at.% Ti, 595 °C in Fe−Ti and 95 at.% Ti, 765 °C in Ni−Ti, is reported to cross all the three vertical sections at a much higher Ti concentration of about 98 at.% Ti and at a temperature in between 670 and 680 °C.

4.2.2. The medium Ti region (∼0.3 < x(Ti) < 0.5)

No experimental results have been found in literature about the solid state equilibria in this region of the phase diagram, except for the cited isothermal sections at 900 and 1000 °C, which show good agreement in this composition range (see Figs. 11 and 12, respectively).

4.2.3. The low-Ti region (x(Ti) < ∼0.3)

This region has been mainly investigated by Van Loo et al. [126], Abramycheva et al. [145] (isothermal sections at 900 and 1000 °C, Figs. 11 and 12, respectively) and Vogel and Wallbaum [143]. Vogel and Wallbaum studied 11 partial vertical sections (at 0.8, 4, 8, 12, and 14.4 wt% Ti, at Fe/Ni weight ratios 90/10 and 40/60, and at Fe/Ti weight ratios 82/18, 78/22, 74/26 and 65/35) in the range delimited by Fe, Ni, Ni_3Ti and Fe_2Ti. Two of these sections are reported in Fig. 14. They also investigated the Ni-rich part of the Ni−Ti binary diagram up to about 35 at.% Ti with results in fair agreement with the presently accepted version of the phase diagram. As for the equilibria reported in the ternary vertical sections they seem reliable as far as the liquid phase is present. Solid state phase equilibria, however, seem less reliable: the sections at Fe/Ni mass ratio equal to 90/10 and 40/60, for instance, are not consistent with the isothermal sections at 900 and 1000 °C [126,145].

These two isothermal sections (see Figs. 11 and 12) show a general good agreement in the composition range

Table 4
Phase compositions of the three phase equilibrium between β-Ti, (Fe,Ni)Ti_2 and (Fe,Ni)Ti at 900 and 1000 °C

	β-Ti			(Ni,Fe) Ti_2			B2-(Fe,Ni)Ti		
	at% Fe	at% Ni	at% Ti	at% Fe	at% Ni	at% Ti	at% Fe	at% Ni	at% Ti
900 °C [126]	~20	~2	~78	~28	~5	~67	~46	~2	~52
1000 °C [145]	20.4	0.1	79.2	30.1	2.4	67.5	45.6	0.7	53.7

considered here. In particular, they suggest an appreciable increase with temperature of the Ti solubility in γ-(Fe,Ni). However, it has to be noted that the s-shaped trend of the Ni_3Ti solubility in γ-(Fe,Ni) reported at 1000 °C [145] is unlikely. A partial isothermal section at 1027 °C was investigated by Drake [151]. The original work being not available, it is reported in Fig. 15 as quoted by Gupta [141]. It seems more accurate than that proposed by Abramycheva et al. [145] either in the Fe-rich corner, where equilibria with α-Fe are present as in the shape of the γ-(Fe,Ni) phase field in equilibrium with Ni_3Ti, which looks more reliable and in good qualitative agreement with the results from Van Loo et al. [126].

Cellular precipitation of Ni_3Ti in γ-(Fe,Ni) was studied by Speich [147] and Fournelle [148] in alloys at 28.7 at.% Ni and 7.0 at.% Ti. Note that Speich [147], relying on the results of Vogel and Wallbaum [143], considered Ni_3Ti metastable (with respect to Fe_2Ti) at such global composition and at 700 °C. According to the isothermal section by Van Loo et al. [126], however, it is an equilibrium phase already at 900 °C at such composition.

4.3. Scheil diagram

Invariant equilibria involving the liquid phase are summarized in the reaction scheme shown in Fig. 16. It is partially based on the work of Vogel and Wallbaum [143] and partially interpolated from the binary equilibria. Invariant equilibria in the solid state, not reported in the diagram, are those involving α-Ti, at high Ti, and $FeNi_3$, in the region close to Fe−Ni.

5. Fe−Ni−Ti thermochemical data

5.1. Experimental measurements

Ostrovskii et al. [152] measured the enthalpy of dissolution of titanium in Fe−Ni melts using high temperature calorimetry for compositions up to 10 at.% Ni and 5 at.% Ti. Their values follow the right tendencies for the partial enthalpies of mixing, but are not in exact agreement with the later results [153,154]. Lück et al. [153] investigated the enthalpy of mixing at 1600 °C in the iron rich part of the Fe−Ni binary and along the section $Fe_{0.89}Ni_{0.11}$−Ti using high temperature calorimetry. The values are shown in Fig. 17. Thiedemann et al. [154] measured the enthalpy of mixing in the Ni−Ti and Fe−Ni−Ti liquid by levitation calorimetry. Their results for the Ni−Ti binary system are in close agreement with previous data in the Ni-rich part and are the only available data in the Ti-rich part. In the ternary system, they performed experiments along part of three lines in the composition triangle (see Fig. 17).

The formation of the R-phase from the B2-phase in a $Ti_{50}Ni_{47}Fe_3$ alloy was studied by Goo and Sinclair [155] and Manosa et al. [136]. By numerical integration of the values of the differential scanning calorimetry measurements, Manosa et al. found that $\Delta H = 0.10$ J/mol and $\Delta S = 0.00042$ J/mol K while Goo et al. found a value of 0.07 J/mol for ΔH.

5.2. Theoretical calculations

By assuming that ternary interactions are not important and by using different extrapolation techniques, Lück et al. [153]

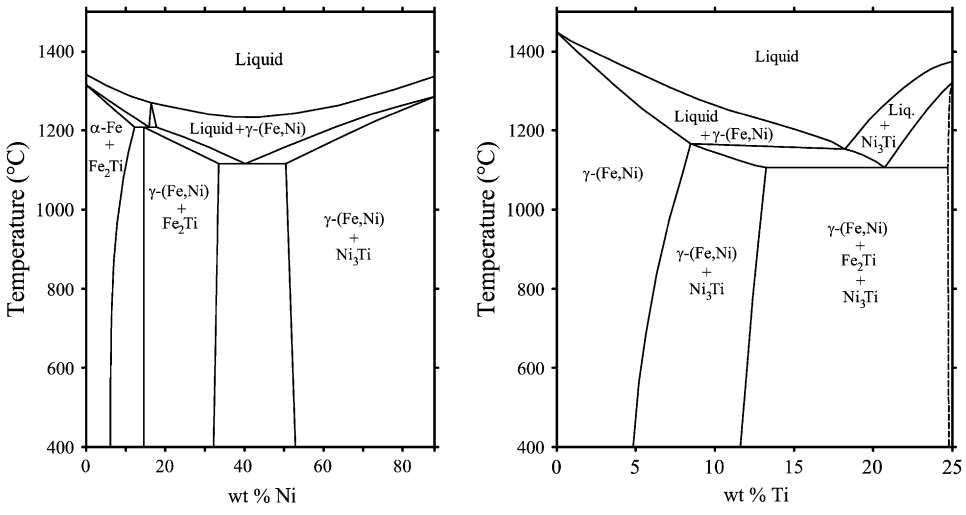

Fig. 14. Selected Fe−Ni−Ti partial vertical sections at 12 wt% Ti (left) and 40/60 Fe/Ti weight ratio (right) according to Vogel and Wallbaum [143].

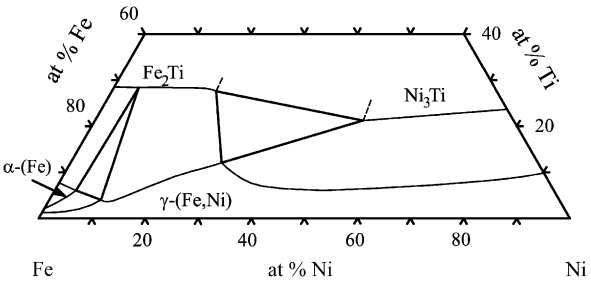

Fig. 15. Fe−Ni−Ti partial isothermal section at 1027 °C according to Drake [151], as quoted by Gupta [141].

could calculate the enthalpy of mixing for the ternary system using only assessments of the binaries. From the comparison between the different techniques, it can be seen that the extrapolations according to Toop and Hillert give the best results for this system. Tomiska and Wang [156] used the Thermodynamic Adapted Power (TAP)-series to fit the data from Lück et al. [153]. This fit has about the same accuracy than the extrapolations from Toop and Hillert, but is only based on best mathematical description of the excess enthalpy of mixing.

In the binary Ni−Ti system Thiedemann et al. [154] could represent their own experimental results conveniently following the regular associate model and considering that associates of composition Ni_3Ti are formed. Assuming no ternary interactions and using previous assessments of the Fe−Ni and Fe−Ti systems, they could reproduce the main features of their results for the ternary system as well as the experimental data from Lück et al. [153]. Fig. 17 shows the enthalpies of mixing according to this description [154] together with the experimental data.

5.3. Calphad modelling

No complete thermodynamic assessment of the ternary system was reported yet. A CALPHAD-type calculation based on the description of binary systems only was done by Miettinen [157]. Ternary parameters were introduced for the liquid and the disordered bcc and fcc phases. This calculation was only meant for steels where the solute contents are quite small. It should be considered as a first approximation.

6. Fe−Ni−Ti atomistic and diffusion data

Bozzolo et al. [158] used the Bozzolo−Ferrante−Smith (BFS) method to study the substitutional site preference of

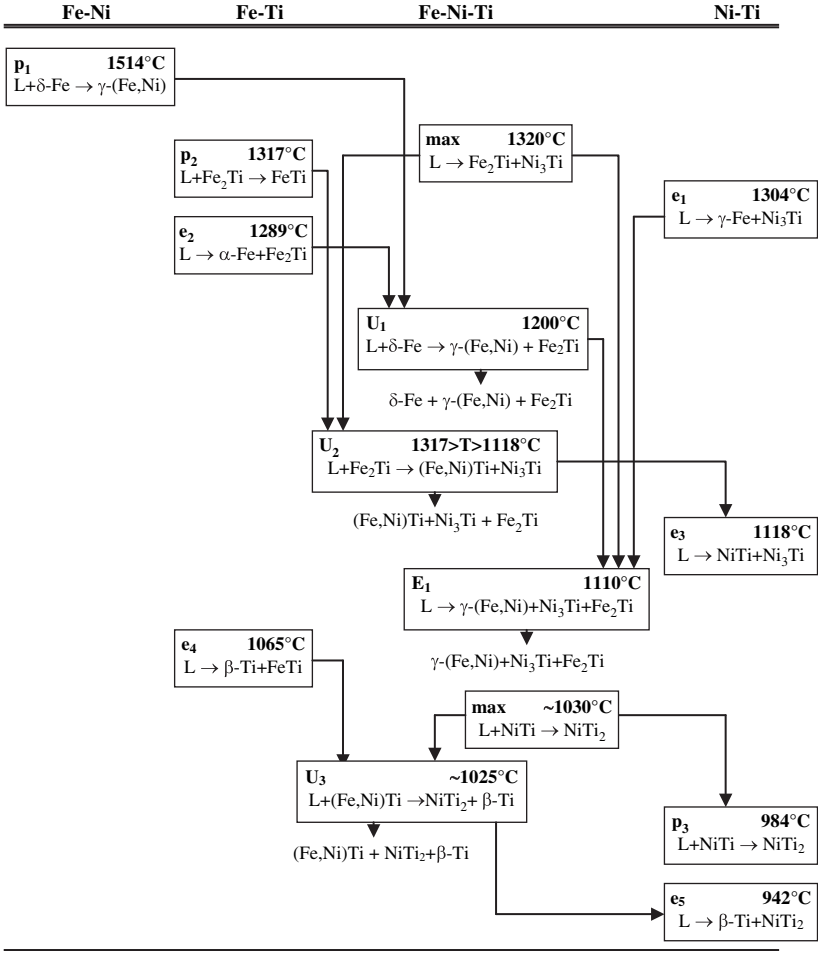

Fig. 16. Partial Fe−Ni−Ti reaction scheme.

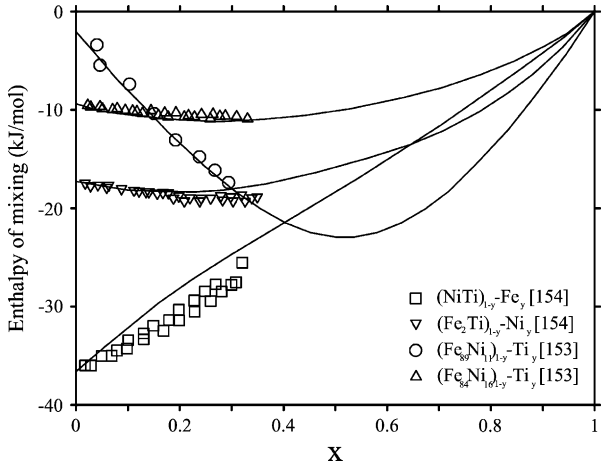

Fig. 17. Enthalpy of mixing of liquid Fe−Ni−Ti alloys. Data points from Lück et al. [153] and Thiedemann et al. [154]; full lines are calculated according to the associate model [154].

Ni additions to FeTi B2 compounds among others. These authors found that Ni partitions to the Fe sublattice rather than to the Ti sublattice. No other atomistic calculations have been so far reported in the ternary Fe−Ni−Ti system.

Diffusion measurements in the ternary Fe−Ni−Ti system are very scarce. Efimenko et al. studied interactions between TiFe and Ni [159] and between Ti_2Ni−Ti eutectic and iron substrate [160], but in the latter no diffusion coefficients were determined.

7. Conclusions

The ternary Fe−Ni−Ti system appears at the same time very simple and poorly known. It is very simple because no ternary phase appears and thermodynamic properties are readily derived from the side binaries (at least for the liquid phase). However, the lack of extended or precise knowledge of phase boundaries and thermodynamic properties appears quite strange owing to the technical importance of the alloys based on Fe, Ni or Ti. It is even more curious to recognize that many of the alloys based on any of these three species contain also both of the two other elements. The present review has stressed the need for further experiments on phase equilibria in the Ti-rich corner, but it should be recognized also that the temperature and composition dependence of the Ti solubility in Fe−Ni alloys are not yet known with a convenient accuracy. A CALPHAD-type assessment of the phase diagram would be highly welcome in that it could (i) help defining critical experiments for a better knowledge of this system; (ii) give the foundation for settling a common data-bank for Fe-, Ni- and Ti-based alloy systems.

Acknowledgements

This work was performed within the frame of the COST ACTION 535 (Thalu) and the partial support of COST-ESF. Italian authors have been partially supported by MIUR, project PRIN2003091235.

References

[1] Bürgel R. Handbuch Hochtemperatur-Werkstofftechnik. Germany: Vieweg; 1998.
[2] Hornbogen E. SFB 316: Verbundwerkstoffe, University of Dortmund, 11−12 Dec 1986.
[3] Guerin G. Key Eng Mater 1995;101−102:339−92.
[4] Hara T, Ohba T, Okunishi E, Otsuka K. Mater Trans JIM 1977;38(1):11−7.
[5] Chu JP, Lai YW, Lin TN, Wang SF. Mater Sci Eng 2000;A277:11−7.
[6] Voronin VI, Naish VE, Novoselova TV, Sagaradze IV. Phys Met Metallogr 2000;89(1):19−26.
[7] Xu H, Jiang C, Gong S, Feng G. Mater Sci Eng 2000;A281:234−8.
[8] Porter DA, Easterling KE. Phase transformations in metals and alloys. London, UK: Chapman & Hall; 1992.
[9] Kurita T, Matsumoto H, Sakamoto K, Tanji K, Abe H. J Alloys Compd 2005;396:193−6.
[10] Zhao C, Liang G, Li C, Jin Z. Scripta Mater 1998;38:1163−8.
[11] Jost N. Metall 1990;44:17−22.
[12] Eggeler G, Hornbogen E, Yawny A. Mater Sci Eng 2004;A378(1−2): 24−33.
[13] Firstov GS, Van Humbeeck J, Koval YN. Mater Sci Eng 2004; A378(1−2):2−10.
[14] Morgan NB. Mater Sci Eng 2004;A378(1−2):16−23.
[15] Schryvers D, Potapov P, Santamarta R. Mater Sci Eng 2004; A378(1−2):11−5.
[16] Li J, Jiang Q, Shen P, Cailiao G. J Funct Mater 1999;30(2):164−5.
[17] Inoue A, Takeuchi A. Mater Trans 2002;43(8):1892−906.
[18] Nishiyama N, Amiya K, Inoue A. Mat Res Soc Symp Proc 2003;806:387−92.
[19] Palmstrom C. MRS Bull 2003;28(10):725−8.
[20] Goldsmid HJ, Nolas GS. Proc Internati Conf on Thermoelectrics, ICT, Proc 2001: p. 1−6.
[21] Nanda BRK, Dasgupta I. J Phys Condens Matter 2003;15:7307−23.
[22] Qiang JB, Wang YM, Wang DH. J Non-Cryst Solids 2004;334−335:223−7.
[23] Bahadur D, Srinivas V, Dunlap RA. J Non-Cryst Solids 1989;109(1):54−8.
[24] Schlapbach L. Hydrogen in intermetallic compounds I+II. Heidelberg: Springer; 1988.
[25] Zuettel M. Mater Today 2003;6(9):24−33.
[26] Oguro K, Osumi Y, Suzuki H, Kato A. J Less Common Met 1983;89:275−9.
[27] Lee SM, Perng TP. J Alloys Compd 1999;291:254−61.
[28] Sagaradze VV, Morozov SV, Shabashov VA, Romashev LN, Kuznetsov RI. Phys Metals Metallogr 1988;66(2):111−20.
[29] Sagaradze VV, Morozov SV. Mater Sci Forum 1992;88−90:147−54.
[30] Swartzendruber LJ, Itkin VP, Alcock CB. J Phase Equilib 1991;12:288−312.
[31] Rossiter PL, Jago RA. Mat Res Soc Symp Proc 1984;21:407−11.
[32] Xing ZS, Gohil DD, Dinsdale AT, Chart T. DMA(A) 103. London: National Physical Laboratory; 1985.
[33] Chuang YY, Chang YA, Schmid R, Lin JC. Metall Trans 1986;A17:1361−72.
[34] Yang CW, Williams DB, Goldstein JI. J Phase Equilib 1996;17:522−31.
[35] Reuter KB, Williams DB, Goldstein JI. Metall Trans A 1989; A20:719−25.
[36] Kakeshita T, Saburi T, Shimizu K. Philos Mag 2000;B80:171−81.
[37] Tupitsa DI, Shabashov AG, Golikov AG. Fiz Met Metalloved 1991;4:127−32.
[38] Munroe PR, Hatherly M. Scripta Metall Mater 1995;32:93−7.
[39] El-Khasan A, Abdel-Aziz K, Vertman AA, Samarin AM. Russ Metall 1966;3:10−6.
[40] Predel B, Mohs R. Arch Eisenhüttenwes 1970;41:143−9.

[41] Tozaki Y, Iguchi YI, Ban-ya S, Fuwa T. Proc Int Symp, London, 1971. The Iron and Steel Institute; 1973. p. 130−2.
[42] Batalin GI, Mineko NN, Sundavtsova VS. Russ Metall 1974;5:82−6.
[43] Iguchi Y, Tozaki Y, Kakizaki M, Fuwa T, Ban-ya S. J Iron Steel Inst Jpn 1981;67:925−32 [in Japanese].
[44] Thiedemann U, Rösner-Kuhn M, Matson DM, Kuppermann G, Drewes K, Flemings MC, et al. Steel Res 1998;69:3−7.
[45] Steiner W, Krisement O. Arch Eisenhüttenwes 1961;37:701−7.
[46] Dench WA. Trans Faraday Soc 1963;59:1279−92.
[47] Kubaschewski O, Stuart LEH. J Chem Eng Data 1967;12:418−20.
[48] Spencer PJ, Hayes FH, Elford L. Proc Int Symp, London, 1971. The Iron and Steel Institute; 1973. p. 322−6.
[49] Speiser R, Jacobs AJ, Spertnak JW. Trans Metall Soc AIME 1959; 215:185−92.
[50] Zellars GR, Payne SL, Morris JP, Kipp RL. Trans Metall Soc AIME 1959;215:181−5.
[51] Onillon M, Olette M. CR. Acad Sci C (Paris) 1966;263:1122−5.
[52] Belton GR, Frueham RJ. J Phys Chem 1967;71:1403−9.
[53] Mills KC, Kinoshita K, Grieveson P. J Chem Thermodyn 1972; 4:581−90.
[54] Kubaschewski O, Geiger KH, Hack K. Z Metallkd 1977;68:337−41.
[55] Conrad BR, Mcaneney TS, Sridhan R. Metall Trans B 1978;9:463−8.
[56] Maruyama N, Ban-ya S. J Jpn I Met 1978;42:992−9.
[57] Rammensee W, Fraser DG. Ber Bunsen-Ges Phys Chem 1981; 85:558−92.
[58] Vrestal J, Pokorna A, Stransky K. Kovové Mater 1974;1:3−9.
[59] Trinel-Dufour CC, Perrot MP. CR. Acad Sci C (Paris) 1975;281: 589−92.
[60] Dalvi AD, Sridhar R. Can Metall Q 1976;15(4):349−57.
[61] Robinson D, Argent BB. Met Sci 1976;10:219−21.
[62] Grimsey EJ, Biswas AK. J Chem Thermodyn 1977;9:415−22.
[63] Ono K, Veda Y, Yamaguchi Y, Moriyama J. T Jpn I Met 1977;18: 610−6.
[64] Hausch G. J Magn Magn Mater 1990;92:87−91.
[65] Seifter A, Pottlacher G, Jager H, Groboth G, Kaschnitz E. Ber Bunsen-Ges Phys Chem 1998;102(9):1266−71.
[66] Chang H, Sastri S, Alexander B. Acta Metall 1980;28(7):925−32.
[67] Rostovtsev RN, Kutsenok IB, Geiderikh VA, Mogutnov BM. Russ J Phys Chem 1990;64(1):139−41.
[68] Chuang YY, Hsieh K, Chang YA. Metall Trans 1986;A17:1373−80.
[69] Lee BJ, Lee DN. Calphad 1988;12:393−403.
[70] Ohnuma I, Kainuma R, Ishida K. CALPHAD and alloy thermodynamics. In: Turchi PEA, Gonis A, Schull RD, editors. TMS; 2002.
[71] Himuro Y, Tanaka Y, Kamiya N, Ohnuma I, Kainuma R, Ishida K. Intermetallics 2004;12:635−43.
[72] Lee BJ. Calphad 1993;17. 251−168.
[73] Howald RA. Metall Mater Trans 2003;A34:1759−69.
[74] Horiuchi T, Igarashi M, Abe F, Mohri T. Calphad 2002;26:591−7.
[75] Mishin Y, Mehl MJ, Papaconstantopoulos DA. Acta Mater 2005;53:4029−41.
[76] Rancourt DG, Dubé M, Heron PRL. J Magn Magn Mater 1993;125: 39−48.
[77] Dubé M, Heron PRL, Rancourt DG. J Magn Magn Mater 1995;147:122−32.
[78] Dang MZ, Rancourt DG. Phys Rev B 1996;53:2291−302.
[79] Jönsson B. Scand J Metall 1994;23:201−8.
[80] Ugaste YE, Kodentsov AA, Van Loo F. Fiz Met Metalloved 1999;88(6):88−94.
[81] Murray JL. Phase diagrams of binary titanium alloys. ASM International; 1987. p. 99−111.
[82] Schön CG. PhD thesis. Düsseldorf; 1998.
[83] Korsunskii IL, Lomonosov VV, Pazhin YuF, Samarin PF, Silakov RS. J Phys Chem Solids 1997;58:361−4.
[84] Yamane T, Hisayuki K, Nakao R, Minamino Y, Araki H, Hirao K. Metall Mater Trans 1999;A30:3009−11.
[85] Yamane T, Hisayuki K. J Mater Sci Lett 2000;19:929−30.
[86] Dong C, Hei ZK, Wang LB, Song QH, Wu YK, Kuo KH. Scripta Metall Mater 1986;20:1155−8.
[87] Jonsson S. Metall Mater Trans 1988;B29:361−70.
[88] Kubaschewski O, Dench WA. Acta Metall 1955;3:339−46.
[89] Fruehan RJ. Metall Trans 1970;1:3403−10.
[90] Wagner S, St. Pierre GR. Metall Trans 1974;5:887−8.
[91] Furukawa T, Kato E. Trans ISIJ 1976;16:382−7.
[92] Esin YO, Valishev MG, Ermakov AF, Geld PV, Petrushevskii MS. Izv Akad Nauk SSSR Met 1981;3:30−2.
[93] Gachon JC, Notin M, Hertz J. Thermochim Acta 1981;48(1−2):155−64.
[94] Gachon JC, Hertz J. Calphad 1983;7:1−12.
[95] Batalin GI, Kurach VP, Sudavtsova VS. Russ J Phys Chem 1984; 58(2):289−91. and. Z Fiz Khim 1984;58:481−3.
[96] Chart TG, Putland FH. NPL Report DMA(A) 96; January 1985.
[97] Wang H, Lück R, Predel B. Z Metallkd 1991;82:659−65.
[98] Wang H, Lück R, Predel B. Z Metallkd 1993;84(4):230−6.
[99] Thiedemann U, Qin JP, Schaefers K, Rösner-Kuhn M, Frohberg MG. ISIJ Int 1995;35(12):1518−22.
[100] Qin JP, Rösner-Kuhn M, Schaefers K, Thiedemann U, Frohberg MG. Z Metallkd 1996;87(4):280−5.
[101] Kaufman L, Nesor H. Calphad 1978;2(1):55−80.
[102] Murray JL. Bull Alloy Phase Diagrams 1981;2:320−34.
[103] Balasubramanian K. Unpublished research. Stockholm: Dept. Materials Science and Engineering, KTH; 1989.
[104] Hari Kumar KC, Wollants P, Delaey L. Calphad 1994;18:223−34.
[105] Rand M.H. COST 507 report; 1998. p. 205−7.
[106] Dumitrescu LFS, Hillert M, Saunders N. J Phase Equilib 1998;19:441−8.
[107] Hari Kumar KC. XXVIII CALPHAD meeting, Grenoble, 2−7/5/1999.
[108] Balun J. PhD thesis. Aachen; 2004.
[109] Inden G. Z Metallkd 1975;66:648−53.
[110] Ohnuma I, Schön CG, Kainuma R, Inden G, Ishida K. Acta Mater 1998;46(6):2083−94.
[111] Eleno LTF, Schön CG, Balun J, Inden G. Z Metallkd 2004; 95(6):464−8.
[112] Nakajima H, Koiwa M, Ono S. Scripta Metall Mater 1983;17:1431−4.
[113] Koiwa M. Mater Trans JIM 1998;39(12):1169−79.
[114] Nakajima H, Ohshida S, Nonaka K, Yoshida Y, Fujita FE. Scripta Mater 1996;34(6):949−53.
[115] Shevchuk YuA. Inorg Mater 2004;40(4):445−9.
[116] Efimenko LP, Petrova LP, Polyakova IG. Russ Metall (Metally) 1997;1:133−8.
[117] Yoshida Y, Masuda Y, Hasslein H, Fujita FE, Nakajima H. Defect Diffus Forum 1997;143:461−6 [part 1].
[118] Klugkist P, Herzig C. Phys Status Solidi A 1995;148(2):413−21.
[119] Kale GB, Patil RV, Gawade PS. J Nucl Mater 1998;257:44−50.
[120] Patil RV, Kale GB, Gawde PS. J Nucl Mater 2001;297:153−60.
[121] Ghosh M, Chatterjee S. Mater Charact 2002;48:393−9.
[122] Ghosh M, Chatterjee S. Mater Sci Eng A 2003;358:152−8.
[123] Murray JL. Phase diagrams of binary nickel alloys. In: Nash P, editor. ASM International; 1991. p. 342−55.
[124] Bellen P, Hari Kumar KC, Wollants P. Z Metallkd 1996;87:972−8.
[125] Abraham JK. Trans Met Soc AIME 1968;242:2365−7.
[126] Van Loo FJJ, Vrolifk JWGA, Bastin GF. J Less Common Met 1981;77:121−30.
[127] Dudkina LP, Kornilov II . Izv Akad Nauk SSSR Met 1967;184(4):184. and Russ Metall 1967;4:98−101.
[128] Shimizu K, Tadaki T. Mater Trans JIM 1992;33(3):165−77.
[129] Tuscher E. Monatsch Chem 1980;111:535−46.
[130] Hwang CM, Meichle M, Salamon MB, Wayman CM. J Phys 1982;43(C4):231−42.
[131] Nishida M, Honma T. J Phys 1982;43(C4):225−30.
[132] Edmonds KR, Hwang CM. Scripta Metall Mater 1986;20(5):733−7.
[133] Rao J, He Y, Ma R. Metall Trans 1990;21A(5):1322−4.
[134] Airoldi G, Otsuka K, Riva G, Sciacca A, Zhang J. Mater Trans JIM 1992;33:730−3.
[135] Ma R, Jianxi R. Philos Mag 1992;65A:123−30.
[136] Manosa L, Rios-Jara D, Ortin J, Planes A, Bohigas X. J Phys Condens Matter 1992;4:7059−66.
[137] Moberly WJ. Diss Abstr Int 1992;52(9):360.
[138] Tadaki T, Shimizu KI, Yamamoto S. Mat Res Soc 1992;246:219−24.

[139] Matveeva NM, Klopotov AA, Kormin NM, Sazanov YuA. Russ Metall 1993;3:216−20.
[140] Gupta KP, Rajendraprasad SB, Jena AK, Sharma RC. J Alloy Phase Diagrams 1985;1:59−68.
[141] Gupta KP. Phase diagrams of ternary nickel alloys, part 1. Indian Institute of Metals; 1990. p. 321−43.
[142] Gupta KP. J Phase Equilib 2001;22(2):171−5.
[143] Vogel R, Wallbaum HS. Arch Eisenhuttenwesen 1938;12:299−304.
[144] Vogel R. Z Metallkd 1941;33:376.
[145] Abramycheva NL, V'yunitskii IV, Kalmykov KB, Dunaev SF. Vestn Mosk Univ Khim 1999;40:139−43.
[146] Alisova SP, Budberg PB, Barmina TI, Lutskaya NV. Russ Metall 1994;1:117−21. and. Izv RAN Metal 1994;1:158−63.
[147] Speich GR. Trans Met Soc AIME 1963;227:754−62.
[148] Fournelle RA. Acta Metall 1979;27:1135−45.
[149] Jia CC, Ishida K, Nishizawa T. Experimental methods of phase diagram determination. In: Morral JE, Schiffman RS, Merchant SM, editors. TMS; 1994. p. 31−8.
[150] Riani P, Cacciamani G, Thebaut Y, Lacaze J. Intermetallics, this issue.
[151] Drake S.C. BSc thesis. MIT; 1982. p. 34.
[152] Ostrovskii OI, Dyubanov VG, Stomakhin AYa, Grigoryan VA. Izv Vyssh Ucheb Zaved Chern Metall 1975;7:67−70.
[153] Lück G, Wang H, Predel B. Z Metallkd 1991;82:805−9.
[154] Thiedemann U, Rösner-Kuhn M, Drewes K, Kuppermann G, Frohberg MG. J Non-Cryst Solids 1999;250−252:329−35.
[155] Goo E, Sinclair R. Acta Metall 1985;33(9):1717−23.
[156] Tomiska J, Wang H. Ber Bunsen-Ges Phys Chem 1995;99(4): 633−40.
[157] Miettinen J. Calphad 1998;22(2):275−300.
[158] Bozzolo GH, Noebeb RD, Amadorc C. Intermetallics 2002;10:149−59.
[159] Efimenko LP, Petrova LP, Sviridov SI. Russ Metall (Metally) 1999;4: 160−5.
[160] Efimenko LP, Petrova LP, Sviridov SI. Russ Metall (Metally) 2000;3: 42−6.
[161] Villars P, Prince A, Okamoto H. Handbook of ternary alloy phase diagrams, vols. 1−2. ASM International; 1995.